Earth and Planetary Science Letters 277 (2009) 244–252

Contents lists available at ScienceDirect

Earth and Planetary Science Letters

journal homepage: www.elsevier.com/locate/epsl

Estimates of the transition zone temperature in a mechanically mixed upper mantle

Jeroen Ritsema [a,*], Wenbo Xu [a], Lars Stixrude [b], Carolina Lithgow-Bertelloni [b]

[a] Department of Geological Sciences, University of Michigan, Ann Arbor, MI 48109, USA
[b] Department of Earth Sciences, University College London, Gower Street, London WC1E 6BT, UK

ARTICLE INFO

Article history:
Received 15 July 2008
Received in revised form 13 October 2008
Accepted 20 October 2008
Available online 29 November 2008

Editor: R.D. van der Hilst

Keywords:
mantle
mechanical mixing
mineral physics
travel times
temperature

ABSTRACT

Partial melting of mantle peridotite generates a physically and chemically layered oceanic lithosphere that is cycled back into the mantle in subduction zones. Stirring times of the mantle are too long to allow for complete re-homogenization of subducted basalt and harzburgite, given the low chemical diffusivity of the solid mantle. This suggests that the Earth's mantle is a mechanical mixture of basaltic and harzburgitic components. Using a recently developed thermodynamic formulism we determine the phase equilibria and the seismic properties of a mantle comprised of a mechanical mixture of basalt and harzburgite (MM) and a homogeneous mantle (EA) with identical pyrolitic bulk chemistry. We use the theoretical shear velocity profiles as a new thermometer of the mantle below the magma-genetic zone by modeling the difference $\Delta T_{410\text{-}660}$ between traveltimes of shear wave reflections off the 410-km and 660-km with the potential temperature T_P. $\Delta T_{410\text{-}660}$ are measured from waveform stacks. They indicate that, over 1000+ km wave lengths, the temperature varies by about 200 K. Lowest and highest temperatures are resolved for the western Pacific subduction zones and the central Pacific, respectively. This variation is similar for the EA and MM and is in excellent agreement with estimates of transition zone thickness and shear velocity variations. The median value of T_P for the EA is 1720 K. It is about 1625 K for the MM, a value that is in better agreement with the Normal-MORB values of 1610±40 K inferred from olivine-liquid equilibria given that our sampling region encompasses the Western Pacific subduction zones and the oldest parts of the Pacific Plate. We argue therefore that a mechanical mixed mantle, with generally higher velocities and steeper velocities gradients, represents a better physical reference model than a model based on a fully equilibrated assemblage.

1. Introduction

Mid-ocean ridges are the major sources of chemical differentiation of the Earth's mantle. Here, the partial (~10–20%) melting of mantle peridotite generates a basaltic crust and leaves behind its depleted complement, harzburgite (McKenzie and Bickle, 1988; Ringwood, 1975). In subduction zones, the physically and chemically layered oceanic lithosphere is cycled back into the mantle. The basaltic crust reaches a depth of at least 150 km (Abers, 2000) and, after transforming to eclogite, its density is higher than the density of harzburgite. Buoyancy forces can produce a radial variation in the amount of subducted crust, including segregation of the basaltic component, toward the base of the mantle (Christensen and Hofmann, 1994; Xie and Tackley, 2004; Brandenburg and van Keken, 2007). Numerical simulations of convection suggest stirring times of the mantle between 250 and 750 million years (Kellogg et al., 2002), which are too long to allow for complete re-homogenization of subducted basalt and harzburgite, given the low chemical diffusivity of the solid mantle (Hofmann and Hart, 1978; Farber et al., 1994). The view that the Earth's mantle is a mechanical mixture of basaltic and harzburgitic components is also supported by geochemistry (Hofmann and White, 1982), field observations (Allègre and Turcotte, 1986), trace element chemistry of basalts (Hofmann and White, 1982; Sobolev et al., 2007), and observations of seismic wave scattering (Cleary and Haddon, 1972; Hedlin et al., 1997; Helffrich, 2006).

So far, the effects of major-element disequilibrium have not been included in joint mineral physics and thermodynamic calculations of the seismic structure of the mantle (Bina and Helffrich, 1992; Ita and Stixrude, 1992; Connolly and Petrini, 2002; Cammarano et al., 2003; Mattern et al., 2005; Stixrude and Lithgow-Bertelloni, 2005a,b). Using the calculations of Xu et al. (2008), we consider the mantle as a mixture of basalt and harzburgite, use the basalt fraction as a metric for the bulk composition, and show that disequilibrium has a profound effect on seismic velocities and shear wave traveltimes through the upper mantle transition zone.. Using new stacks of shear wave reflections off upper mantle discontinuities we estimate the temperature variation in the upper mantle and demonstrate that the average temperature in the mantle may be overestimated by nearly 100 K if disequilibrium is ignored.

2. Homogeneous and mechanically mixed compositions of the mantle

Following our recent study (Xu et al., 2008), we invoke two end-member models for combining basalt and harzburgite in the mantle.

* Corresponding author.
E-mail address: jritsema@umich.edu (J. Ritsema).

0012-821X/$ – see front matter © 2008 Elsevier B.V. All rights reserved.
doi:10.1016/j.epsl.2008.10.024

Table 1
Bulk composition in mol % (from Xu et al., 2008)

Component	Pyrolite[a]	Basalt[a]	Harzburgite[b]
SiO_2	37.82	46.06	36.02
MgO	48.72	13.30	56.51
FeO	6.03	6.28	5.97
CaO	2.87	13.35	0.79
Al_2O_3	4.34	18.14	1.30
Na_2O	0.21	3.87	0.00

[a] (Workman and Hart, 2005).
[b] (Baker and Beckett, 1999).

The Equilibrium Assemblage (EA) has perfect re-equilibration and the Mechanical Mixture (MM) has complete disequilibrium between the basalt and harzburgite fractions. The phase assemblage for the EA of homogeneous pyrolite is defined as

$$\Psi(fX_B + (1-f)X_H). \quad (1)$$

The phase assemblage for the MM of basalt and harzburgite is defined as

$$f\Psi(X_B) + (1-f)\Psi(X_H). \quad (2)$$

Here, Ψ describes the phase proportions given the bulk compositions of basalt, X_B, and harzburgite, X_H, and a basalt fraction f. Equilibrium phase assemblages, isentropic temperature, physical properties of coexisting phases, seismic velocities (including elastic and anelastic effects) and density are computed using the thermodynamic approach of Stixrude and Lithgow-Bertelloni (2005a,b) and Xu et al. (2008).

The Depleted Mid-Ocean-Ridge-Basalt Mantle (DMM) of Workman and Hart (2005) was used as the reference estimate of the bulk composition, and we approximated the composition of basalt, X_B as the MORB model of Workman and Hart (2005) and the composition of harzburgite, X_H, as the most depleted composition of abyssal peridotites from Baker and Beckett (1999) (Table 1). A basalt fraction, f_B, of 18% produces the DMM composition, consistent with estimates by Morgan and Morgan (1999) and Sobolev et al. (2007). The major-element chemistry is comprised of six components: CaO, FeO, Al_2O_3, MgO, SiO_2, Na_2O, 20 phases, and 45 mantle species (Xu et al., 2008).

Fig. 1 shows phase diagrams computed for the EA and MM. As demonstrated by Xu et al. (2008), proportions of mantle minerals in the EA and the MM are different. For example, the olivine fraction at low pressure in the EA is about 56%, but it is about 65% in the MM. The garnet-pyroxene fraction is higher in the EA and free silica, which is stable in the basalt fraction, is present only in the MM. Since the expected phase stabilities of the EA and the MM differ, their seismological properties of the upper mantle differ. This is demonstrated in Fig. 2 for a range of potential temperatures and basalt fractions f. Xu et al. (2008) have discussed in detail the seismological consequences of mechanical mixing, including absolute seismic velocities and velocity gradients, densities, and the velocity increases and sharpness of the 410-km and 660-km seismic discontinuities. Here, we emphasize two that are most relevant to shear wave traveltimes in the upper mantle.

First, the shear wave velocity in the MM is about 0.06 km/s higher than in the EA due to the lower proportion of low-velocity phases, such as clinopyroxene and the presence of stishovite, a high-velocity mantle phase. The shear velocity in MM has a steeper radial velocity gradient in the deeper parts of the transition zone because of the relatively high proportions of the high-velocity phases wadsleyite, ringwoodite, and akimotoite, and the lower proportion of garnet. The shear velocity in the transition zone (410–660 km depth) for the MM does not depend on basalt fraction.

Second, both the EA and MM present the temperature dependence of seismic velocities and the depth of phase transitions in the olivine fraction. The shear velocity is lower and higher in a relatively warm and cold upper mantle, respectively. The olivine-to-wadsleyite transition (at the 410-km) is elevated in a relatively cold upper mantle (such as in subduction zones) while the ringwoodite-to-perovskite and ringwoodite-to-ferropericlase transitions are lowered, thereby thickening the transition zone. In relatively warm (upwelling) regions opposite deflections of the 410-km and 660-km will produce thinner transition zones (Bina and Helffrich, 1994).

3. Upper mantle shear wave reflections

Using theoretical shear velocity profiles for the EA and the MM, we investigate the effects of mechanical mixing on the traveltimes of shear waves through the upper mantle transition zone, where velocity structure and depths of the 410-km and 660-km depend strongly on temperature. Shear wave reflections are ideal phases for the study of the transition zone. Shear wave reflections (*SdS*) are underside reflections from a seismic discontinuity at depth d (Fig. 3). They arrive with predictable

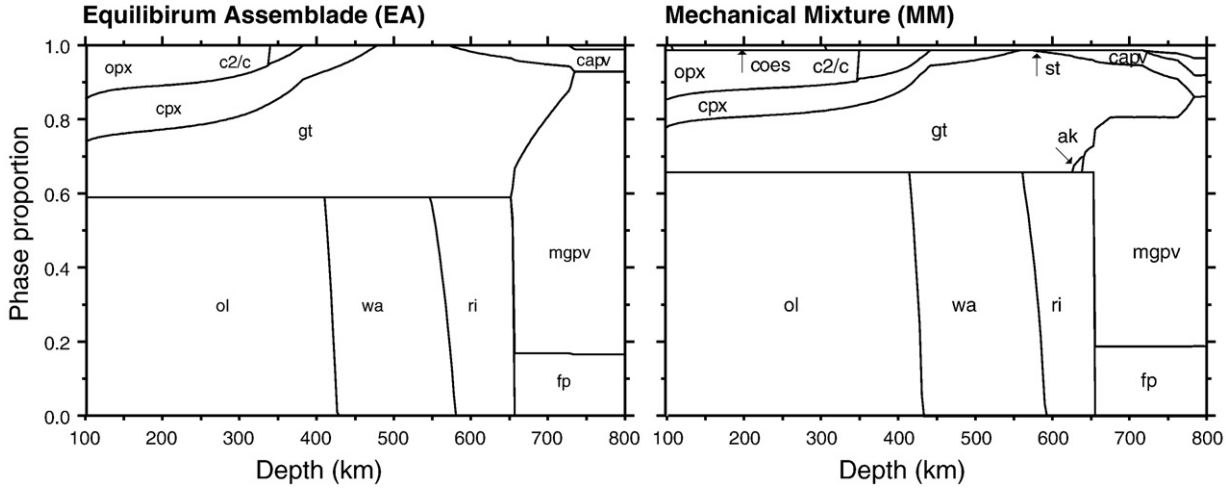

Fig. 1. Phase diagrams for (left) a chemically equilibrated mantle (EA) and (right) a mechanically mixed (MM) mantle with identical pyrolitic composition with a basalt fraction f=20% and an adiabatic geotherm with a potential temperature of 1600 K. Indicated phases are: plagioclase (pl), orthopyroxene (opx), high pressure Mg-rich clinopyroxene (c2/c), clinopyroxene (cpx), garnet (gt), akimotoite (ak), olivine (ol), wadsleyite (wa), ringwoodite (ri), stishovite (st), Ca-silicate perovskite (capv), Mg-rich silicate perovskite (mgpv), and ferropericlase (f_P) (modifed from Xu et al., 2008).

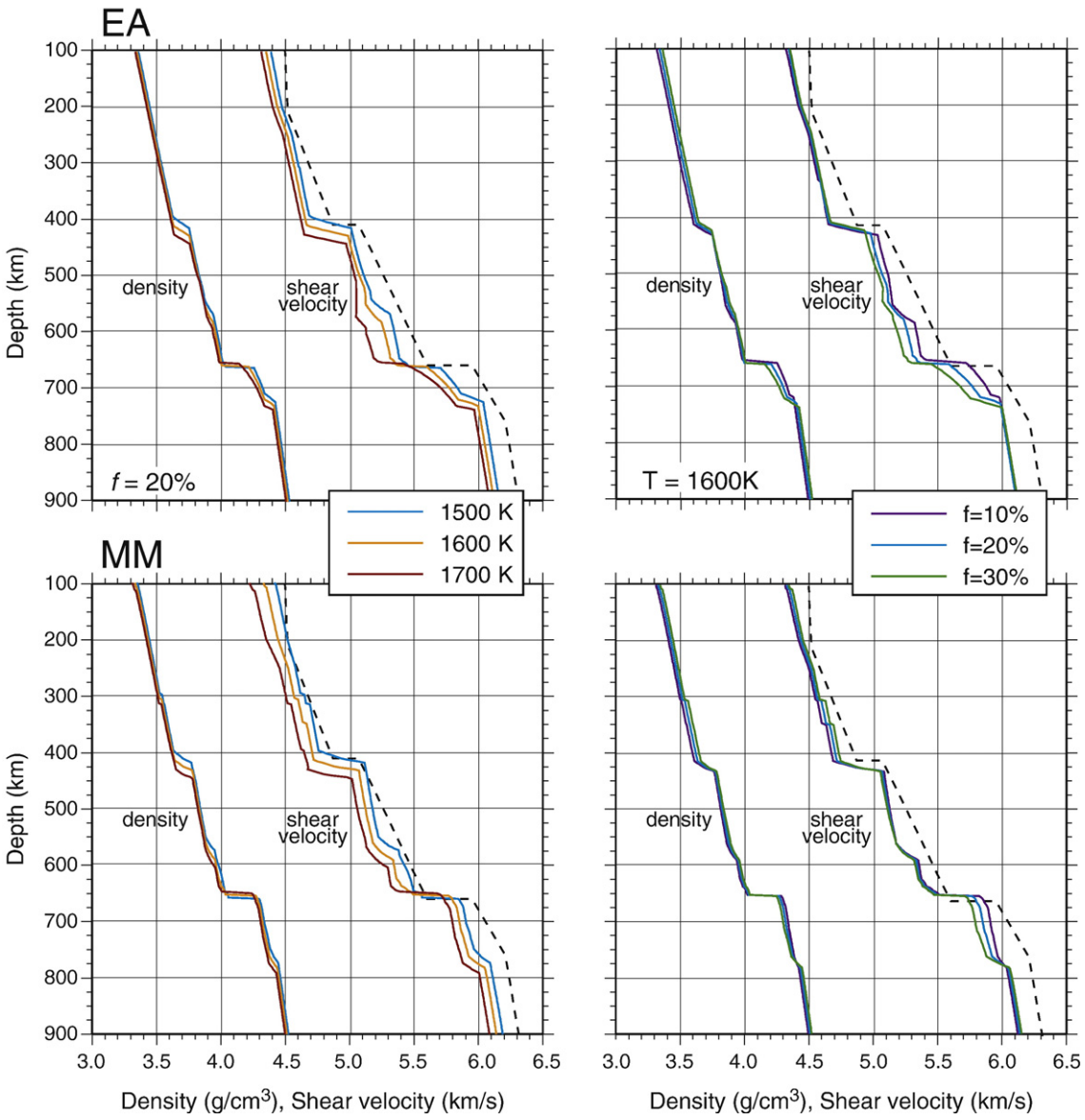

Fig. 2. Profiles of shear wave velocity and density as a function of depth for the (top) Equilibrium Assemblage (EA) and (bottom) the Mechanical Mixture (MM). Profiles on the left are computed for a basalt fraction f=20% and adiabatic geotherms with potential temperatures of 1500 K, 1600 K, and 1700 K. Profiles on the right are computed for an adiabat with a potential temperature of 1600 K and basalt fractions f of 0.1, 0.2, and 0.3. The IASP91 shear velocity profile is drawn with a dashed line.

arrival times and slownesses relative to the major phase SS and are well recorded in long-period (T>5–10 s) seismograms (Shearer, 1991). S410S and S660S, in particular, are recorded with relatively high amplitudes. S410S and S660S arrive about 150 s and 230 s before SS and their amplitudes are about 3–4% of the SS amplitude, respectively. Their differential traveltime $\Delta T_{410\text{-}660}$ is insensitive to crustal and uppermost mantle structure and it has a coherent geographic variation (Shearer and Masters, 1992).

Previous analyses of $\Delta T_{410\text{-}660}$ have focused on estimating the variable transition zone thickness whereby global scale tomography models have been used to infer wave speeds in the transition zone (Flanagan and Shearer, 1999; Gu and Dziewonski, 2002; Schmerr and Garnero, 2007; Houser et al., 2008). Our approach here is fundamentally different. We will use mineral physics based calculations of upper mantle shear velocity (e.g., Fig. 2) to compute $\Delta T_{410\text{-}660}$ and compare these directly to values measured using broadband waveforms. The theoretical models incorporate the effects of pressure, temperature, and composition on both shear wave velocities and phase transition depths in a self-consistent manner. It is therefore straightforward to model $\Delta T_{410\text{-}660}$ using temperature as modeling variable without invoking a-priori corrections for variations in seismic velocity in the transition zone.

3.1. Data sets

Our data set is comprised of global and regional network recordings of shallow (<50 km) earthquakes (1985–2007) with magnitudes between Mw=6.0–7.4. The data have been retrieved from the Incorporated Research Institutions for Seismology (IRIS) Data Management System

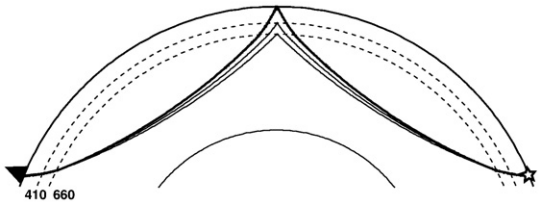

Fig. 3. Ray geometrical paths of (thick line) SS and (thin lines) S410S and S660S. Dashed lines indicate the 410-km and 660-km discontinuities.

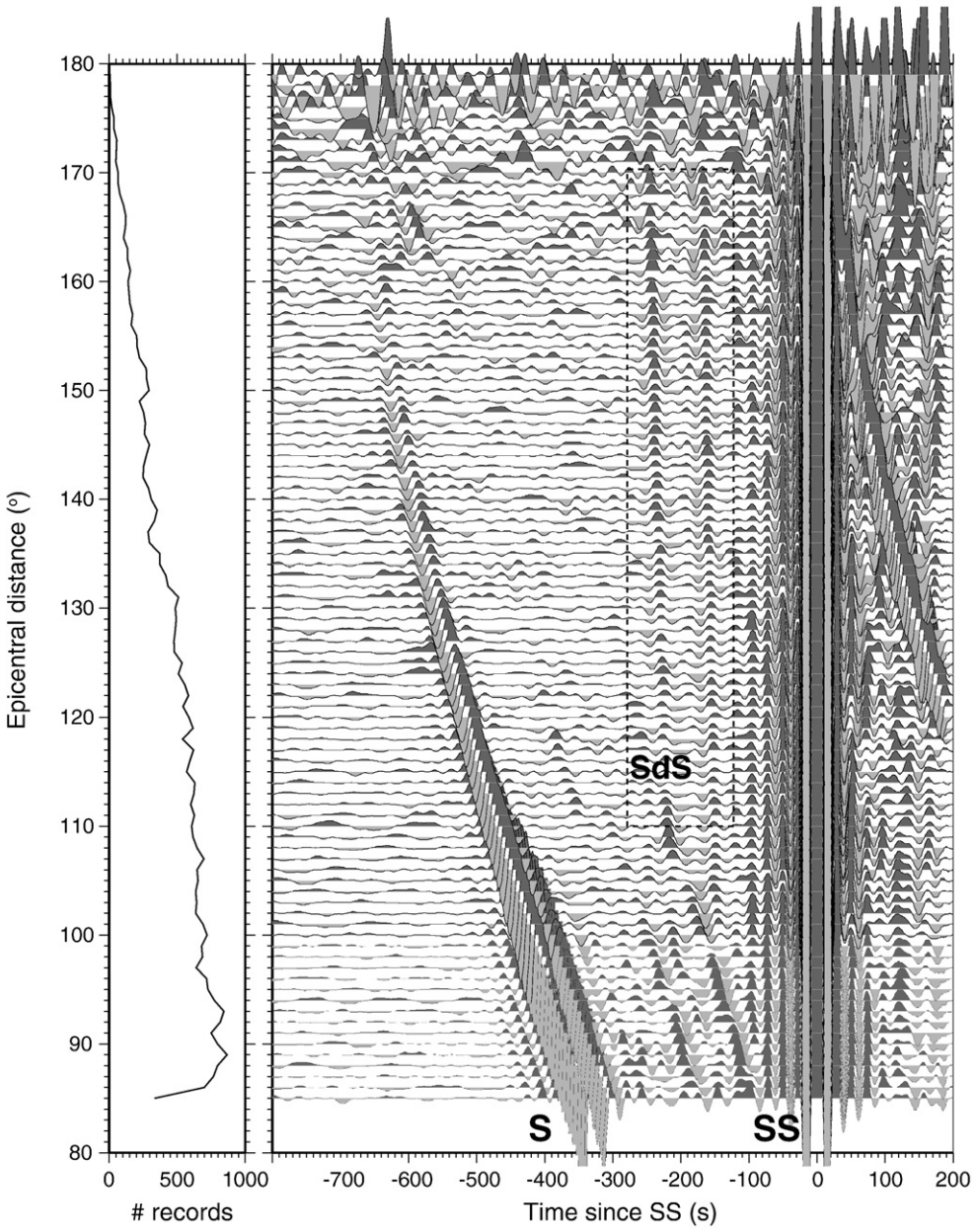

Fig. 4. Record section of global shear wave recordings summed in epicentral distance bins of 1°. The number of records in each sum is indicated on the left. Major phases (Sdiff, SS) are indicated. The S*d*S reflections off upper mantle discontinuities arrive with the regions indicated by the dashed lines. The phases S410S and S660S are clearly visible.

and the GEOSCOPE Data Center. The waveforms are corrected for sensor response and rotated into vertical, radial and transverse components. We analyze the SS data using the transverse component waveforms (Fig. 4). The waveforms are band-pass filtered between 8 and 100 mHz to suppress low and high frequency noise. A total of 37,000 selected waveforms have simple, high-amplitude SS phases and signals between S and SS with amplitudes that are at least a factor of 3 lower than SS. The waveforms are normalized so that the SS phases have positive polarities and peak amplitudes equal to 1. By waveform correlation, the waveforms are shifted to maximize the alignment of SS. Waveform segments with predictable arrivals (e.g., Ss*d*s, ScS*d*ScS) are smoothly tapered to zero within 20-s long windows (Schmerr and Garnero, 2006).

3.2. Waveform stacking

To bring out the relatively low-amplitude upper mantle reflections from incoherent noise, we form data stacks $S^D(x_0, t)$ for subsets of waveforms which have ray-theoretical SS surface reflection points that fall within circular caps with radii of 10° (Flanagan and Shearer, 1999; Gu and Dziewonski, 2002; Schmerr and Garnero, 2007). Summation using these broad averaging regions mimics the averaging effects due to the broad Fresnel zone of the SS wave (Choy and Richards, 1975) and it ensures that we include a sufficient number of waveforms in the sum to suppress incoherent noise. The stacks are computed for a grid of x_0 with a spacing of 5°. Prior to summation, distance dependent time shifts $\Delta T(\Delta,x)$ are applied to align S*d*S reflections off horizontal upper mantle discontinuities at a depth of d km. $\Delta T(\Delta,x)$ is computed using iasp91 ray-theoretical traveltimes (Crotwell et al., 1999; Kennett and Engdahl, 1991). Move-out corrections depend little on the chosen 1D reference model. Waveforms with lowest noise level, defined by the average absolute amplitude in a 200-s long window between S and SS level, are given highest weight in the summation. Uncertainties in the traveltimes and amplitudes are determined by bootstrapping (Efron and Tibshirani, 1986).

The highest quality stacks (Fig. 5) have been determined for x_0 within the Pacific and circum Pacific regions of the northern

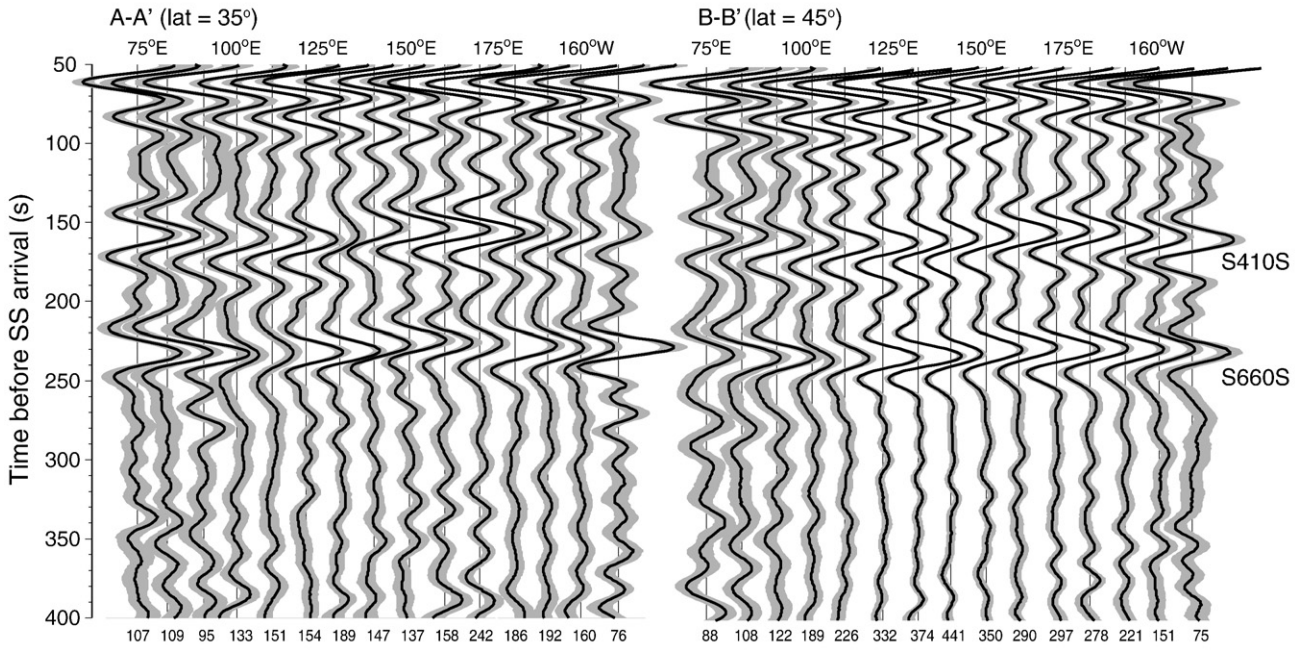

Fig. 5. Stacks $S^D(x_0, t)$ along cross-section A–A′ and B–B′ (see Fig. 6). The reflections from the 660-km and 660-km arrive around 157 s and 230 s before SS (according to the iasp91 model). The shaded regions represent the 95% confidence bounds of the amplitude of $S^D(x_0, t)$, based on bootstrapping analysis. The number of traces used in each stack is indicated below.

hemisphere where most SS reflections points are located (Fig. 6). Reflections from the 410-km and 660-km discontinuity have the highest amplitudes (3–4% of the SS amplitude). Reflections from a depth of 220 km arrive about 80 s before SS and interfere with large initial downswings in front of SS. The 520-km discontinuity, arriving between S660S and S410S (Deuss and Woodhouse, 2001; Shearer, 1990), can only be recognized above the 95% confidence bounds in few stacks.

Synthetics stacks $S^M(x_0, t)$ are computed by summing reflectivity synthetics (Fuchs and Muller, 1971), computed for an earthquake at a depth of 20 km and a source mechanism with favorable teleseismic SS radiation. The synthetics (Fig. 7) show systematic variations in S660S and S410S traveltime as function of temperature and basalt fraction. For both the EA and the MM, the traveltime between SS and S410S increases and $\Delta T_{410\text{-}660}$ decreases for increasing temperature, due to the increasing delay of SS in the upper mantle and the decreasing width of the transition zone, respectively. Due to these competing effects, the traveltime between SS and S660S increases only slightly with increasing temperature. Changes in the basalt fraction *f* do not significantly affect $\Delta T_{410\text{-}660}$ for the MM since transition zone velocities are unaffected by variation in *f*. For the EA, $\Delta T_{410\text{-}660}$ increases for increasing *f* due to decreased transition zone velocities. However, for realistic basalt fractions ($f<30\%$) $\Delta T_{410\text{-}660}$ is primarily affected by temperature. S520S is substantially smaller due to the relatively small impedance contrast

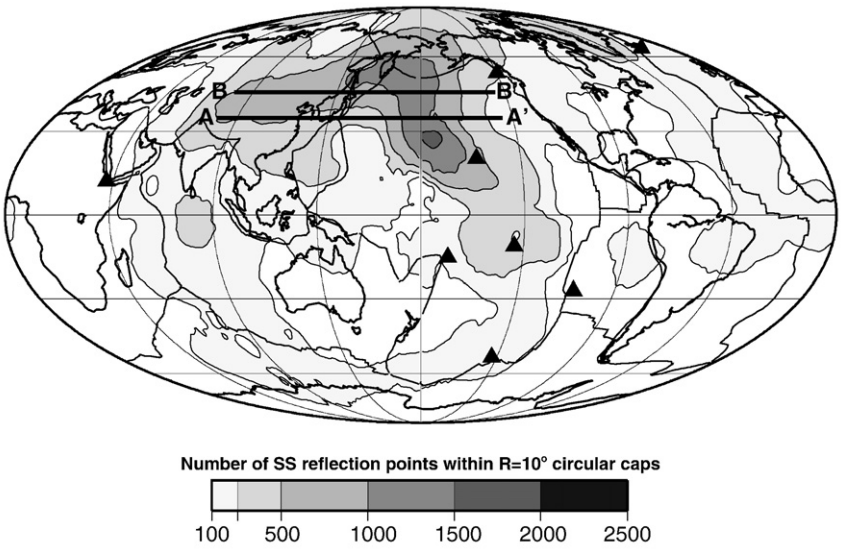

Fig. 6. Number of SS surface reflection points for the global waveform set used in this study. Lines A–A′ and B–B′ are parallels at 35°N and 45°N, respectively, and extend from 70°E to 140°W. Triangles are hotpot location from the compilation of Ritsema and Allen (2003).

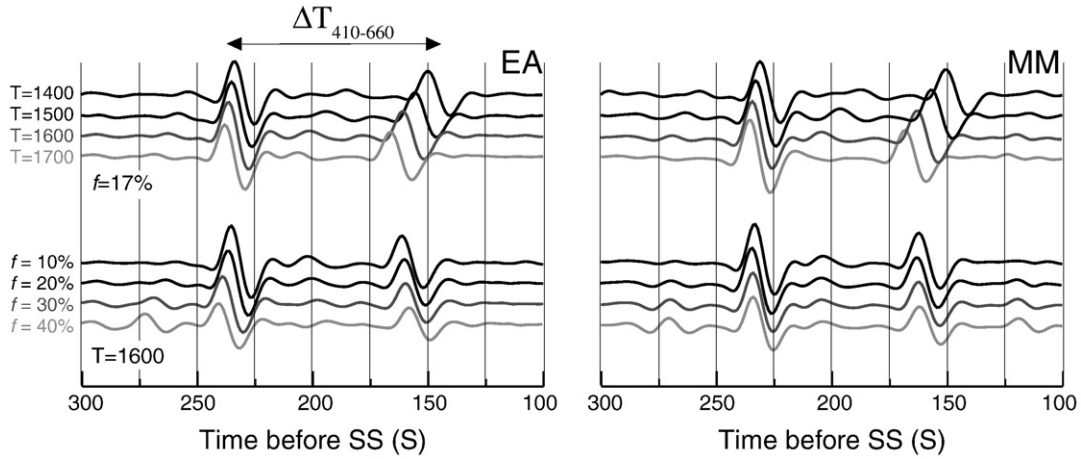

Fig. 7. Synthetic shear waveforms for (left) EA and (right) MM for (top) potential temperatures of 1400 K, 1500 K, 1600 K, and 1700 K (for a constant basalt fraction $f = 17\%$) and for (bottom) basalt fractions $f = 10\%$, $f = 20\%$, $f = 30\%$, and $f = 40\%$ (for a constant potential temperature of 1600 K). The waveforms are calculated for a distance of 130°. A 200-s long portion of the SS precursory window with upper mantle *SdS* reflections is shown. The largest signals are S660S (at ~230 s) and S410S (at ~160 s).

between wadsleyite and ringwoodite. It becomes weaker with increasing temperature, which may explain why it is not observed globally (Lawrence and Shearer, 2006; Shearer, 1996).

To produce synthetics stacks, the same data processing steps have been applied to the synthetics. The band-pass filtered synthetics have SS phases with equalized amplitude of 1 and they have been aligned by waveform correlation. Although we use a single source mechanism, a stack $S^M(x_0, t)$ includes synthetic waveforms with the same epicentral distribution as the waveforms used to produce $S^D(x_0, t)$ so that artifacts due to inhomogeneous slowness sampling are reproduced.

4. Results

For each data stack $S^D(x_0, t)$ we measure the traveltime difference $\Delta T_{660\text{-}410}$ between S410S and S660S by correlating their waveforms. While our data set has global coverage, we observe that the highest precision measurements are obtained for stacks comprised of at least 75 waveforms. In these stacks S410S and S660S signals have similar waveforms well above noise level and vary little when processing parameters are varied. Therefore, the most robust measurements apply to the transition zone beneath the Pacific and circum-Pacific in the northern hemisphere (Fig. 6).

We measure $\Delta T_{660\text{-}410}$ for the synthetics stacks $S^{\mathbf{M}}(x_0, t)$ in the same manner. The synthetic stacks are computed for potential temperatures T_P between 1400 K and 1800 K with a 50 K interval and a fixed basalt fraction of 17%. Since $\Delta T_{660\text{-}410}$ varies smoothly, it is straightforward to determine T_P by linear interpolation. We determine T_P for each cap location x_0 such that $\Delta T_{660\text{-}410}$ measured in the data stacks $S^D(x_0, t)$ matches the $\Delta T_{660\text{-}410}$ in the stacks of synthetics $S^M(x_0, t)$.

Fig. 8 shows the distribution of T_P. For both the EA and the MM, T_P varies by about 200 K with an obvious long-wavelength pattern that is in excellent agreement with previous studies of transition zone structure (Fig. 8B): T_P is lowest in the Western Pacific subduction zones where the transition zone is thickest (Shearer and Masters, 1992; Flanagan and Shearer, 1999; Gu and Dziewonski, 2002) and has highest shear velocities (Gu et al., 2001; Ritsema et al., 2004).

Small differences in the variation of T_P for the EA and MM reflect the small differences in the dependence of transition zone velocities on temperature, but overall, the patterns of T_P are similar since the 410-km and 660-km discontinuity depths in the EA and the MM depend on temperature similarly. However, within the sampling region, the average potential temperature for the EA is 1720 K. The average potential temperature for the MM is nearly 100 K lower at 1625 K. This difference is due to the fact that transition zone shear velocities in the MM are higher than in the EA.

5. Discussion and conclusions

By correlating mineralogical models to model seismological data provides a straightforward means to test the properties of the geophysical structure of the upper mantle. We test directly the match of body wave traveltimes to 1D profiles of seismic velocity, computed by calculating the phase equilibria of an upper mantle for simple reference models characterized by pyrolitic compositions and adiabatic geotherms. The calculations provide an effective measure of the temperature in the mantle below the magma-genetic zone, as they predict the elastic properties of the entire mineral assemblage for a specified geotherm in a self-consistent manner. The calculations include the effects of pressure and temperature on the relatively abrupt transformations in the olivine fraction (that produce the 410-km and 660-km discontinuities) and the gradual transformations in the pyroxene and garnet components (that are partially responsible for enhanced shear velocity gradients in the upper mantle).

In this paper we considered the effects of mechanical mixing in the mantle, given the observations of prevalent small-scale geochemical and structural heterogeneity in the upper mantle, low mantle solid-state diffusion rates, and relatively slow mantle convection times. Two end-member models represented a fully re-equilibrated mantle (EA) with a homogeneous pyrolitic composition and a fully mechanically mixed (MM) mantle comprised of harzburgite and basalt (the products of partial melting at mid ocean ridges) with the same pyrolitic bulk chemistry as the EA model. The phase equilibria for the MM and EA are different and consequently their seismic properties are different. Most notably, the MM features higher shear velocities and steeper velocity gradients in the transition zone.

We computed traveltimes of the phases S410S and S660S, which are shear wave reflections off the 410-m and 660-km discontinuities. Their traveltime difference $\Delta T_{660\text{-}410}$ is a robust measure of the ratio of the thickness and the shear velocity in the transition zone (the region between the 410-km and the 660-km). This seismic observable is an excellent indicator of transition zone temperature. Estimates of temperature obtained by modeling $\Delta T_{660\text{-}410}$ differ for the EA and the MM. Since transition zone shear velocities are higher in the MM, its transition zone must be thicker, and hence, its temperature must be lower than in the EA to explain a given observed value $\Delta T_{660\text{-}410}$.

For our sampling region, we obtain an average potential temperature of 1625 K when using the MM. This temperature estimate falls within the temperature range of 1610±40 K for a normal mantle as estimated by Herzberg et al. (2007) and Shen and Forsyth (1995) on the basis of olivine thermometry of Normal-MORB and melting

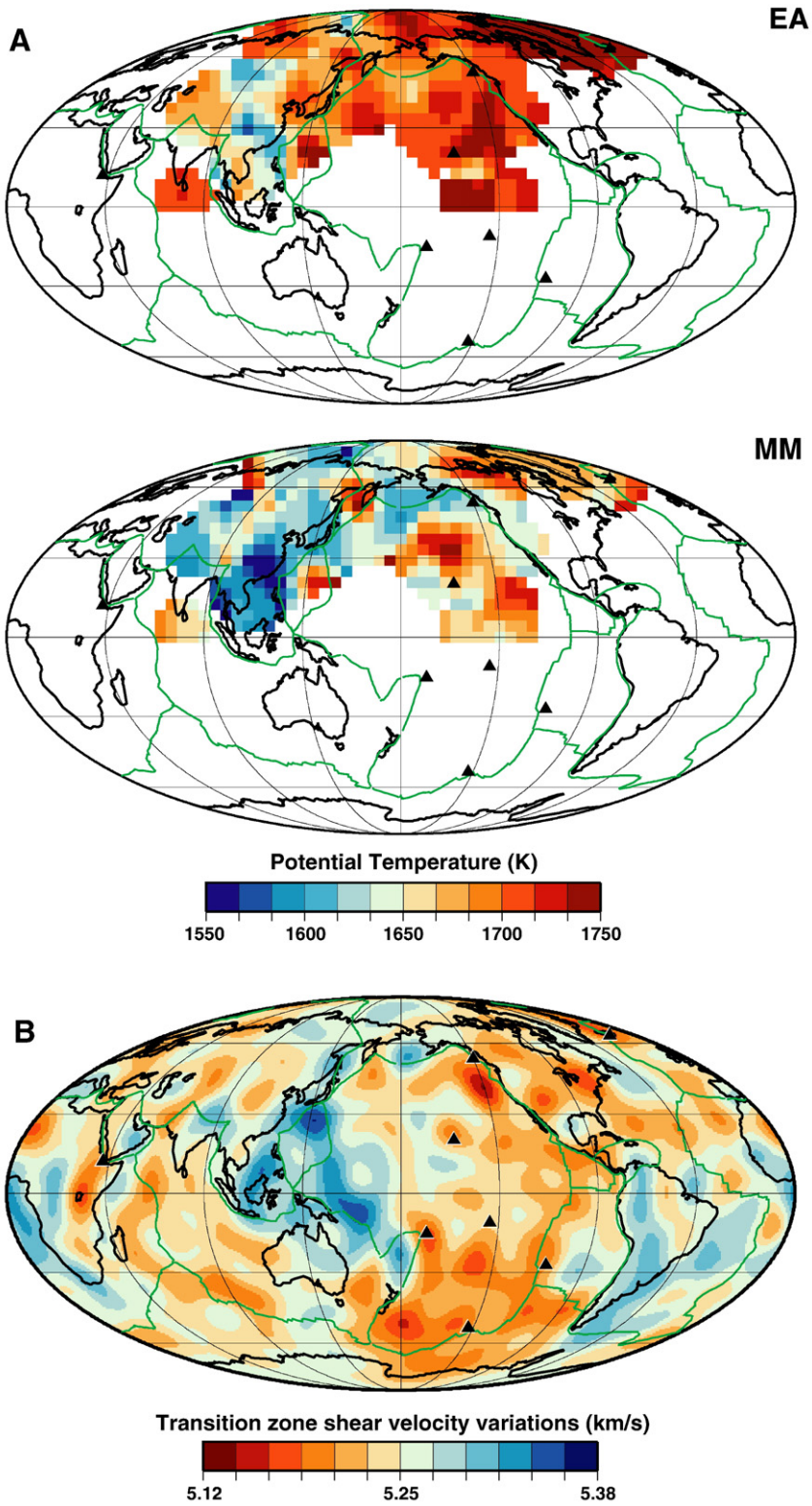

Fig. 8. (A) Estimates of the potential temperature from the modeling of $\Delta T_{410\text{-}660}$ with predictions using synthetic stacks for (top) the Equilibrium Assemblage (EA) and (bottom) a mechanical mixture (MM) of basalt and harzburgite. (B) Shear velocity variation at a depth of 520 km depth according to model S20RTS (Ritsema et al., 1999). Triangles are hotpot location from the compilation of Ritsema and Allen (2003).

initiation depths beneath mid-ocean ridges. The average potential temperature of 1720 K inferred for the EA appears irreconcilable with the petrological estimates of the average mantle temperature given that our sampling region encompasses the relatively cool Western Pacific subduction zones and large portions of the oldest Pacific Plate.

Indeed, both the absolute values of transition zone shear wave velocity and the shear wave gradients for the MM match global 1D shear wave profiles (such as IASP91 or PREM) much better than the EA. Discrepancies may be due to the uncertain effects of majorite on shear velocity (Irifune et al., 1998), the presence of sub-adiabatic

geotherms, or increased concentrations of harzburgite-rich material in the transition zone (Fukao et al., 2001; Cammarano et al., 2005; Nakagawa and Buffett, 2005) that we have ignored in our modeling. Nevertheless, we argue that seismic profiles based on a mechanical mixture of harzburgite and basalt serve as useful 1D physical reference models for further detailed modeling.

The large-scale variation in temperature of about 200 K is dominated by low temperatures in the upper mantle beneath subduction zones and high temperatures beneath the Pacific. The inferred temperature variation correlates well with previous maps of transition zone thickness and maps of seismic shear velocity in the transition zone, indicating that $\Delta T_{660\text{-}410}$ is indeed primarily thermally controlled. The variation is smaller than expected given excess temperatures for mid-plate volcanoes estimated from MgO and FeO content of volcanic rocks (Herzberg et al., 2007; Putirka, 2008) and geophysical estimates of temperature in narrow slabs (Billen and Hirth, 2007) and plumes (Lin and van Keken, 2006). This mismatch can be explained by the large cap-averaging regions that we use in our modeling and by the large Fresnel zones of SS reflections (Neele and Snieder, 1992).

Some second order features in the temperature maps correlate with the shear velocity anomalies in the transition zone. For example, low-temperature anomalies (with respect to subduction zones) beneath Kamchatka and the Central Philippines Plate correlate with high shear velocity anomalies, but in general the correlation is imperfect. In particular, temperature highs are not observed at the Bowie and Hawaii hotspots, which are overlying low shear velocity structures in the transition zone (Ritsema and Allen, 2003). In fact, the strongest high-temperature anomaly in the Pacific is located north of the Hawaii hotspot, far from the inferred location of the Hawaiian plume conduit in the deep mantle (Steinberger and O'Connel, 1998). While a comparison between the temperature and shear velocity is complicated by differences in the map resolution, it is also likely that compositional variation is responsible for the mismatch at the shorter scale lengths.

Acknowledgments

We thank the reviewers for constructive reviews. Data have been provided by the IRIS Data Management Center and the Geoscope Data Center. This research has been funded by the NSF Grant EAR 0609763.

References

Abers, G.A., 2000. Hydrated subducted crust at 100–250 km depth. Earth Planet. Sci. Lett. 176, 323–330.
Allègre, C.J., Turcotte, D.L., 1986. Implications of the two-component marble-cake mantle. Nature 323, 123–127.
Baker, M.B., Beckett, J.R., 1999. The origin of abyssal peridotites; a reinterpretation of constraints based on primary bulk compositions. Earth Planet. Sci. Lett. 171, 49–61.
Billen, M.I., Hirth, G., 2007. Rheologic controls on slab dynamics. Geochem. Geophys. Geosys. 8. doi:101029/2007GC001597.
Bina, C.R., Helffrich, G., 1992. Calculation of elastic properties from thermodynamic equation of state principles. Annu. Rev. Earth Planet. Sci. 20, 527–549.
Bina, C.R., Helffrich, G., 1994. Phase transition Clapeyron slopes and transition zone seismic discontinuity topography. J. Geophys. Res. 99, 15,853–815,860.
Brandenburg, J.P., van Keken, P.E., 2007. Deep storage of oceanic crust in a vigorously convecting mantle. J. Geophys. Res. 112. doi:10.1029/2006JB004813.
Cammarano, F., Goes, S., Vacher, P., Giardini, D., 2003. Inferring upper-mantle temperatures from seismic velocities. Phys. Earth Planet. Inter. 138, 197–222.
Cammarano, F., Goes, S., Deuss, A., Giardini, D., 2005. Is a pyrolitic adiabatic mantle compatible with seismic data? Earth Planet. Sci. Lett. 232, 227–243.
Choy, G.L., Richards, P.G., 1975. Pulse distortion and Hilbert transformation in multiply reflected and refracted body waves. Bull. Seismol. Soc. Am. 65, 55–70.
Christensen, U.R., Hofmann, A.W., 1994. Segregation of subducted oceanic crust and the convecting mantle. J. Geophys. Res. 99, 19,867–819,884.
Cleary, J.R., Haddon, R.A.W., 1972. Seismic wave scattering near the core-mantle boundary: a new interpretation of precursors to PKP. Nature 240, 549–551.
Connolly, J.A.D., Petrini, K., 2002. An automated strategy for calculation of phase diagram sections and retrieval of rock properties as a function of physical condition. J. Metamorph. Geol. 20, 697–708.
Crotwell, H.P., Owens, T.J., Ritsema, J., 1999. The TauP toolkit; flexible seismic travel-time and ray-path utilities. Seismol. Res. Lett. 70, 154–160.
Deuss, A., Woodhouse, J., 2001. Seismic observations of splitting of the mid-transition zone discontinuity in Earth's mantle. Science 294, 354–357.
Efron, B., Tibshirani, R., 1986. Bootstrap methods for standard errors, confidence intervals, and other measures of statistical accuracy. Stat. Sci. 1, 54–75.
Farber, D.L., Williams, Q., Ryerson, F.J., 1994. Diffusion in Mg (sub 2) SiO (sub 4) polymorphs and chemical heterogeneity in the mantle transition zone. Nature 371, 693–695.
Flanagan, M.P., Shearer, P.M., 1999. A map of topography on the 410-km discontinuity from PP precursors. Geophys. Res. Lett. 26, 549–552.
Fuchs, K., Muller, G., 1971. Computation of synthetics seismograms with the reflectivity method and comparison with observations. Geophys. J. R. Astron. Soc. 23, 417–433.
Fukao, Y., Widiyantoro, S., Obayashi, M., 2001. Stagnant slabs in the upper and lower mantle transition region. Rev. Geophys. 39, 291–324.
Gu, Y.J., Dziewonski, A.M., 2002. Global variability of transition zone thickness. J. Geophys. Res. 107, 17.
Gu, Y.J., Dziewonski, A.M., Su, W., Ekstrom, G., 2001. Models of the mantle shear velocity and discontinuities in the pattern of lateral heterogeneities. J. Geophys. Res. 106, 11,169–111,199.
Hedlin, M.A.H., Shearer, P.M., Earle, P.S., 1997. Seismic evidence for small-scale heterogeneity throughout the Earth's lower mantle. Nature 387, 145–150.
Helffrich, G., 2006. Heterogeneity in the mantle; its creation, evolution and destruction. Tectonophysics 416, 23–31.
Herzberg, C., Asimow, P.D., Arndt, N., Niu, Y., Lesher, C.M., Fitton, J.G., Cheadle, M.J., Saunders, A.D., 2007. Temperatures in ambient mantle and plumes: constraints from basalts, picrites, and komatiites. Geochem. Geophys. Geosys. 8. doi:10.1029/2006GC001390.
Hofmann, A.W., Hart, S.R., 1978. An assessment of local and regional isotopic equilibrium in the mantle. Earth Planet. Sci. Lett. 38, 44–62.
Hofmann, A.W., White, W.M., 1982. Mantle plumes from ancient oceanic crust. Earth Planet. Sci. Lett. 57, 421–436.
Houser, C., Masters, G., Flanagan, M., Shearer, P., 2008. Determination and analysis of long-wavelength transition zone structure using SS precursors. Geophys. J. Int. 174, 178–194. doi:10.1111/j.1365-246X.2008.03719.x.
Irifune, T., Higo, Y., Inoue, T., K., Y., O., H., F., K., 1998. Sound velocities of majorite garnet and the composition of the mantle transition zone. Nature 451. doi:10.1038/nature06551.
Ita, J., Stixrude, L., 1992. Petrology, elasticity and composition of the mantle transition zone. J. Geophys. Res. 97, 6849–6866.
Kellogg, J.B., Jacobsen, S.B., O'Connell, R.J., 2002. Modeling the distribution of isotopic ratios in geochemical reservoirs. Earth Planet. Sci. Lett. 204, 183–202.
Kennett, B.L.N., Engdahl, E.R., 1991. Traveltimes for global earthquake location and phase identification. Geophys. J. Int. 105, 429–465.
Lawrence, J.F., Shearer, P.M., 2006. Constraining seismic velocity and density for the mantle transition zone with reflected and transmitted waveforms. Geochem. Geophys. Geosys. 7. doi:10.1029/2006GC001339.
Lin, S.-C., van Keken, P.E., 2006. Dynamics of thermochemical plumes: 2. Complexity of plume structures and its implications for mapping of mantle plumes. Geochem. Geophys. Geosys. 7. doi:10.1029/2005GC001072.
Mattern, E., Matas, J., Ricard, Y., Bass, J.D., 2005. Lower mantle composition and temperature from mineral physics and thermodynamic modeling. Geophys. J. Int. 160, 973–990.
McKenzie, D., Bickle, M.J., 1988. The volume and composition of melt generated by extension of the lithosphere. J. Petrol. 29, 625–679.
Morgan, J.P., Morgan, W.J., 1999. Two-stage melting and the geochemical evolution of the mantle; a recipe for mantle plum-pudding. Earth Planet. Sci. Lett. 170, 215–239.
Nakagawa, T., Buffett, B.A., 2005. Mass transport mechanism between the upper and lower mantle in numerical simulations of thermochemical mantle convection with multicomponent phase changes. Earth Planet. Sci. Lett. 230, 11–27.
Neele, F.P., Snieder, R., 1992. Topography of the 400 km discontinuity from observations of long-period P400P phases. Geophys. J. Int. 109, 670–682.
Putirka, K., 2008. Excess temperatures at ocean islands: implications for mantle layering and convection. Geology 36, 283–286. doi:10.1130/G24615A.
Ringwood, A.E., 1975. Composition and Petrology of the Earth's Mantle. McGraw-Hill, New York.
Ritsema, J., Allen, R.M., 2003. The elusive mantle plume. Earth Planet. Sci. Lett. 207, 1–12.
Ritsema, J., van Heijst, H.J., Woodhouse, J.H., 1999. Complex shear wave velocity structure imaged beneath Africa and Iceland. Science 286, 1925–1928.
Ritsema, J., Van Heijst, H.J., Woodhouse, J.H., 2004. Global transition zone tomography. J. Geophys. Res. 109, B02302.
Schmerr, N., Garnero, E., 2006. Investigation of upper mantle discontinuity structure beneath the Central Pacific using SS precursors. J. Geophys. Res. 111. doi:10.1029/2005JB004197.
Schmerr, N., Garnero, E.J., 2007. Upper mantle discontinuity topography from thermal and chemical heterogeneity. Science 318, 623–626.
Shearer, P.M., 1990. Seismic imaging of upper-mantle structure with new evidence for a 520-km discontinuity. Nature 344, 121–126.
Shearer, P.M., 1991. Constraints on upper mantle discontinuities from observations of long-period reflected and converted phases. J. Geophys. Res. 96, 18,147–118,182.
Shearer, P.M., 1996. Transition zone velocity gradients and the 520-km discontinuity. J. Geophys. Res. 101, 3053–3066.
Shearer, P.M., Masters, T.G., 1992. Global mapping of topography on the 660-km discontinuity. Nature 355, 791–796.
Shen, Y., Forsyth, D.W., 1995. Geochemical constraints on initial and final depths of melting beneath mid-ocean ridges. J. Geophys. Res. 100, 2211–2237.
Sobolev, A.V., Hofmann, A.W., Kuzmin, et al., 2007. The amount of recycled crust in sources of mantle–derived melts. Science 316, 412–417.

Steinberger, B., O'Connel, R.J., 1998. Advection of plumes in mantle flow: implications for hotspot motion, mantle viscosity and plume distribution. Geophys. J. Int. 132, 412–434.
Stixrude, L., Lithgow-Bertelloni, C., 2005a. Mineralogy and elasticity of the oceanic upper mantle: origina of the low-velocity zone. J. Geophys. Res. 110, B03204.
Stixrude, L., Lithgow-Bertelloni, C., 2005b. Thermodynamics of mantle minerals – I. Physical properties. Geophys. J. Int. 162, 610–632.
Workman, R.K., Hart, S., 2005. Major and trace element composition of the depleted MORB mantle (DMM). Earth Planet. Sci. Lett. 231, 53–72.
Xie, S., Tackley, P.J., 2004. Evolution of helium and argon isotopes in a convecting mantle. Earth Planet. Sci. Lett. 146, 417–439.
Xu, W., Lithgow-Bertelloni, C., Stixrude, L., Ritsema, J., 2008. The effect of bulk composition and temperature on mantle seismic structure. Earth Planet. Sci. Lett. doi:10.1016/j.epsl.2008.08.012.